Research Article

Dark Matter Halo as a Source of Regular Black-Hole Geometries

R. A. Konoplya[1], **Alexander Zhidenko**[2]

1. Research Centre for Theoretical Physics and Astrophysics, Institute of Physics, Silesian University in Opava, Opava, Czech Republic; 2. Centro de Matemática, Computação e Cognição (CMCC), Universidade Federal do ABC, Brazil

We construct exact black hole solutions free of curvature singularities, sourced by dark matter halos described by galactic density profiles. Regularity of the geometry is ensured by adopting the relation $P_r = -\rho$ between radial pressure and density, which is consistent with the phenomenological freedom of halo models. In particular, the sufficiently dense Einasto and Dehnen-type profiles for the dark matter halo can produce asymptotically flat solutions of singularity-free black holes embedded in the galactic environment. The resulting regular black holes surrounded by dark matter are shown to be stable under axial perturbations. We further compute the shadow radii and Lyapunov exponents associated with the photon circular orbits around these black holes.

Corresponding author: A. Zhidenko, olexandr.zhydenko@ufabc.edu.br

I. Introduction

The resolution of singularities predicted by classical general relativity remains one of the central challenges in black-hole physics. According to the singularity theorems, geodesic incompleteness is inevitable under broad physical assumptions, suggesting that classical black holes conceal regions where the known laws of physics break down. A wide variety of approaches have been developed to avoid singularities, ranging from quantum-gravity inspired modifications of Einstein's equations to effective models in which exotic matter sources regularize the geometry[1][2][3]. A key question in all such constructions is whether the required matter sources can be justified within astrophysical settings.

On the other hand, black holes in nature are never isolated but always reside in astrophysical environments dominated at large scales by dark matter. Overwhelming observational evidence supports the existence of galactic and cluster dark matter halos[4][5], although the microscopic nature of dark

matter remains unknown. Phenomenological halo models, such as the Hernquist, Navarro–Frenk–White (NFW), and other profiles[6][4], are widely used in galactic dynamics and cosmological simulations. Importantly, these models prescribe the density distribution without fixing a unique relation between pressure and density, thereby leaving freedom for effective fluid descriptions.

In this work we exploit this freedom to construct exact black hole solutions sourced by dark matter halos, focusing on the Einasto Einasto[7] and Dehnen-type Dehnen[8] density profiles. Regular black hole configurations associated with the Dehnen-type profile, which was referred to as the Dekel-Zhao profile[9][10], were recently reviewed in Kar and Kar[11], with particular emphasis on solutions with infinite asymptotic mass. The barotropic subclass of such configurations was also discussed in Sajadi *et al.*[12][13].

In the present study, we establish the general criteria and delineate the characteristic features of density profiles that give rise to regular black-hole geometries. We show that assuming the radial pressure satisfies $P_r = -\rho$ leads to spherically symmetric spacetimes that are everywhere regular and asymptotically flat, with horizons forming under suitable parameter conditions. Within this framework, we obtain a new family of exact solutions describing regular black holes immersed in galactic halos for a broad class of density profiles. In particular, we derive explicit and remarkably simple analytic asymptotically flat black-hole metrics for the Dehnen-type and Einasto distributions in specific parameter ranges. Since the phenomenological profiles specify only the density, our choice of pressure does not conflict with halo phenomenology, while ensuring regularity of the interior. The resulting solutions can be interpreted as singularity-free black holes embedded in galactic environments. We will also show that the obtained configuration of the regular black hole and halo is stable against axial gravitational perturbations of spacetime. As a basic geometry probe of the obtained spacetime, we calculate the shadow radii for several representative examples of regular black holes.

The work is organized as follows. In Section II we formulate the general approach for constructing regular black-hole geometries sourced by spherically symmetric dark-matter distributions. Sections III and IV present explicit examples of such solutions, respectively, for the Einasto and Dehnen-type density profiles. The stability of the obtained configurations under axial perturbations is analyzed in Section V. The shadows cast by the obtained black holes and the Lyapunov exponents for null circular geodesics are considered in Section VI. In Section VII we discuss the physical interpretation and astrophysical relevance of these results, while the main conclusions are summarized in Section VIII.

II. Spherically symmetric dark matter distributions and generic regular black hole solutions

Galactic matter is usually modeled by an anisotropic fluid with some density distribution, which implies an almost spherical halo dominated by dark matter[14]. Depending on the size, mass, and form of a galaxy one or another distribution is preferable.

In order to simplify notations we employ the general form for the spherically symmetric line element,

$$ds^2 = -f(r)dt^2 + \frac{B^2(r)}{f(r)}dr^2 + r^2(d\theta^2 + \sin^2\theta d\varphi^2), \tag{1}$$

where we assume that $B(r) > 0$.

It is convenient to introduce the mass function, $m(r) \leq r/2$, such that

$$1 - \frac{2m(r)}{r} \equiv \frac{f(r)}{B^2(r)}. \tag{2}$$

The horizon radius r_0 satisfies

$$f(r_0) = 0, r_0 = 2m(r_0). \tag{3}$$

The external matter is the anisotropic fluid, so that the nonzero components of the corresponding stress-energy tensor are

$$\begin{aligned} T_t^t &= -8\pi\rho(r), \\ T_r^r &= 8\pi P_r(r), \\ T_\theta^\theta = T_\varphi^\varphi &= 8\pi P(r). \end{aligned} \tag{4}$$

After some algebra, the Einstein equations are reduced to the following form:

$$m'(r) = 4\pi r^2 \rho(r), \tag{5}$$

$$B'(r) = 4\pi r^2 B(r) \frac{\rho(r) + P_r(r)}{r - 2m(r)}. \tag{6}$$

One can notice that, since $B(r_0)$ is finite, Eq. (6) implies the additional condition at the horizon

$$\rho(r_0) + P_r(r_0) = 0. \tag{7}$$

In Konoplya and Zhidenko[15] this condition for zero radial pressure, $P_r(r) = 0$, yielded a modification in the density profile in such a way that $\rho(r_0) = 0$.

In the present paper we do not modify the density profile of dark matter. Instead, we consider the vacuum equation of state[16],

$$P_r(r) = -\rho(r), \tag{8}$$

which automatically satisfies Eq. (7). While this condition is more naturally associated with dark energy than with dark matter on cosmological scales, several studies have explored fluids obeying $p = -\rho$, or approaching this limit in certain regimes, as possible unified descriptions of dark matter and dark energy[17][18][19][20]. Related concepts arise in models of vacuum-like or self-interacting dark matter, in which the dark component effectively behaves as a cosmological-constant term within overdense regions or compact objects[21][22]. It should be emphasized, however, that in our context this equation of state is assumed to hold only within a central part of a galaxy.

Then, it follows from Eq. (6) that

$$B(r) = 1, \tag{9}$$

and we find that the tangential pressure is given

$$P(r) = -\frac{r}{2}\rho'(r) - \rho(r), \tag{10}$$

satisfying the weak energy condition as long as $\rho(r) > 0$ and $\rho'(r) < 0$.

Finally, we can solve Eq. (5),

$$m(r) = 4\pi \int_0^r x^2 \rho(x) dx, \tag{11}$$

where we assume that $m(0) = 0$. In this case there is no singularity in the spacetime as long as the density is finite everywhere.

Thus, in the present paper, we consider density profiles that possess the following features:

1. Monotonically decreasing and nonnegative:

$$\forall r \geq 0 : \qquad \rho(r) \geq 0, \rho'(r) < 0, \tag{12}$$

   which ensures that the weak energy condition is satisfied.

2. Finite everywhere:

$$\forall r \geq 0 : \qquad \rho(r) < \infty, \tag{13}$$

   which guarantees that the corresponding spacetime solution is free of singularities, in particular at $r = 0$.

3. Asymptotically convergent: We also assume that the integral in Eq. (11) converges as $r \to \infty$,

$$\int_0^\infty x^2 \rho(x) dx < \infty. \tag{14}$$

   It should be noted that not all density profiles used to describe galactic halos satisfy this condition,

since realistic galaxies have finite size and typically follow different distribution laws outside their boundaries. In this work, we do not consider such piecewise-defined profiles.

III. Einasto profile

An example of a density distribution obeying all the above conditions is the Einasto profile Einasto[23]; Einasto and Haud[24]; Retana-Montenegro *et al.*[25]:

$$\rho(r) = \rho_0 \exp\left[-\left(\frac{r}{h}\right)^{1/n}\right], n > 0, \tag{15}$$

where ρ_0 is the density in the center, which is expressed in terms of the total mass

$$M = m(r \to \infty) = 4\pi h^3 n \Gamma(3n) \rho_0. \tag{16}$$

Having in mind a scenario in which supermassive galactic black holes could be formed during a long period of time as a result of merging of many smaller black holes, consideration of the Einasto profile does not sound completely exotic. It is shown in Baes[26] that only the Einasto index $n \geq 1/2$ can be supported by an isotropic orbital structure. The Einasto profile Einasto[23]; Einasto and Haud[24] has become one of the most successful empirical descriptions of dark-matter halos, accurately reproducing the smooth curvature of the density slope seen in dynamical simulations Merritt *et al.*[27]; Navarro *et al.*[28]; Springel *et al.*[29]; Acharyya *et al.*[30]. Subsequent works established its close connection to the Sérsic law for stellar systems and related the profile's shape parameter to the halo's mass-accretion history Graham *et al.*[31]; Ludlow *et al.*[32].

It is worth emphasizing that the Einasto profile defines only the density and leaves the pressure profile undetermined. In particular, there is no intrinsic equation of state associated with the Einasto model, since the relation between pressure and density depends on the chosen dynamical description of the halo (e.g., collisionless particles with velocity dispersion governed by the Jeans equations, or an effective fluid approximation). Therefore, adopting the condition $P_r(r) = -\rho(r)$ for the radial pressure is not in conflict with the standard assumptions underlying the Einasto halo, but rather represents a phenomenological choice that ensures regularity of the black hole solution while remaining consistent with the absence of a fixed pressure–density relation in the halo model.

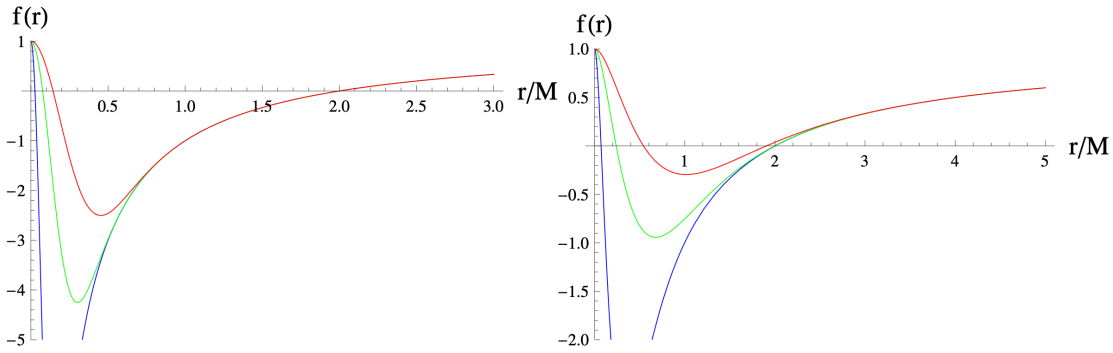

Figure 1. Metric functions for the black hole solutions with Einasto profile $n = 1/2$ (left panel) and $n = 1$ (right panel): $h = 0.1M$ (blue), $h = 0.2M$ (green), and $h = 0.3M$ (red).

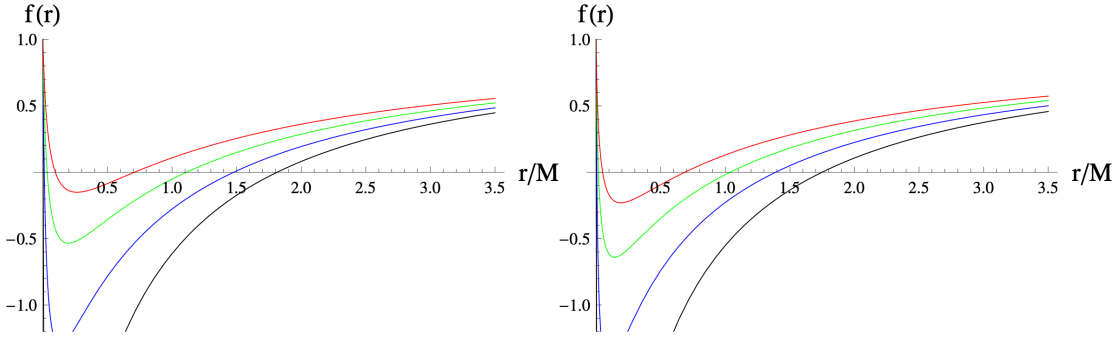

Figure 2. Metric functions for the black hole solutions with Einasto profile for large n.Left panel ($n = 6$): $h = 10^{-8}M$ (black), $h = 2 \cdot 10^{-8}M$ (blue), $h = 3 \cdot 10^{-8}M$ (green), and $h = 4 \cdot 10^{-8}M$ (red).Right panel ($n = 7$): $h = 2 \cdot 10^{-10}M$ (black), $h = 4 \cdot 10^{-10}M$ (blue), $h = 6 \cdot 10^{-10}M$ (green), and $h = 8 \cdot 10^{-10}M$ (red).

Using the above general procedure, we now consider several examples of density profiles that lead to regular black hole solutions. In certain cases, these profiles admit simple analytic expressions, while in the general case the mass function must be obtained numerically by evaluating the corresponding integral. Both analytic and numerical examples are presented below. The accompanying Mathematica® notebook[11]1The Mathematica® notebook is publicly available from https://arxiv.org/src/2511.03066v1/anc/BHEinasto.nb. provides the code for generating solutions for arbitrary values of the profile parameters.

- For $n = 1/2$ we have

$$f(r) = 1 - \frac{2m(r)}{r} = 1 - \frac{2M}{r}\,\mathrm{erf}\left(\frac{r}{h}\right) + \frac{4Me^{-r^2/h^2}}{\sqrt{\pi}h}, \tag{17}$$

where $\mathrm{erf}(z)$ is defined as

$$\mathrm{erf}(z) \equiv \frac{2}{\sqrt{\pi}}\int\limits_0^z e^{-x^2}\,dx,$$

and the asymptotic mass is given by

$$M = \pi^{3/2}\rho_0 h^3. \tag{18}$$

The metric (17) has the event horizon and inner horizon for sufficiently small $h \lesssim 1.05M$.

The Ricci scalar is regular everywhere

$$R = \frac{16Me^{-r^2/h^2}\left(2h^2 - r^2\right)}{\sqrt{\pi}h^5}, \tag{19}$$

as well as the Kretschmann scalar, which has a cumbersome form, though for small r, we find:

$$R_{\mu\nu\lambda\sigma}R^{\mu\nu\lambda\sigma} = \frac{512M^2}{3\pi h^6} - \frac{512M^2r^2}{\pi h^8} + \mathcal{O}(r)^4.$$

- For $n = 1$ the metric takes the following form:

$$f(r) = 1 - \frac{2m(r)}{r} = 1 - \frac{2M}{r} + M\frac{2h^2 + 2hr + r^2}{h^2 r}e^{-r/h}, \tag{20}$$

where

$$M = 8\pi\rho_0 h^3. \tag{21}$$

Again, the metric (20) has the event horizon and inner horizon for sufficiently small $h \lesssim 0.388M$. The Ricci scalar and Kretschmann scalar are regular

$$R = Me^{-r/h}\frac{4h - r}{h^4}, \tag{22}$$

$$R_{\mu\nu\lambda\sigma}R^{\mu\nu\lambda\sigma} = \frac{8M^2}{3h^6} - \frac{20M^2r}{3h^7} + \mathcal{O}(r)^2.$$

- For other values of n one can calculate the integral (11) numerically. Then, studying various numerical solutions at different values of the parameters, we observe that the black hole solutions exist only for sufficiently dense profiles, corresponding to small values of h. The maximum value of h/M, for which the event horizon exists, decreases with n.

For small n, the halo density decreases fast and the black-hole metric outside the horizon deviates from the Schwarzschild geometry only slightly, unless h is sufficiently close to its extreme value (see Fig. 1). Similar black-hole geometries have been recently obtained by introducing Gaussian nonlocality in the radial coordinate of the Schwarzschild metric Boos[33].

For large n the Einasto density profile must be very dense and decays relatively slowly. Therefore, the black-hole metric is significantly different from the Schwarzschild geometry within the parametric range of h providing the existence of the event horizon (see Fig. 2). As a result for larger n the shadow radius and Lyapunov exponents generally differ more from their Schwarzschild values (see Fig. 3).

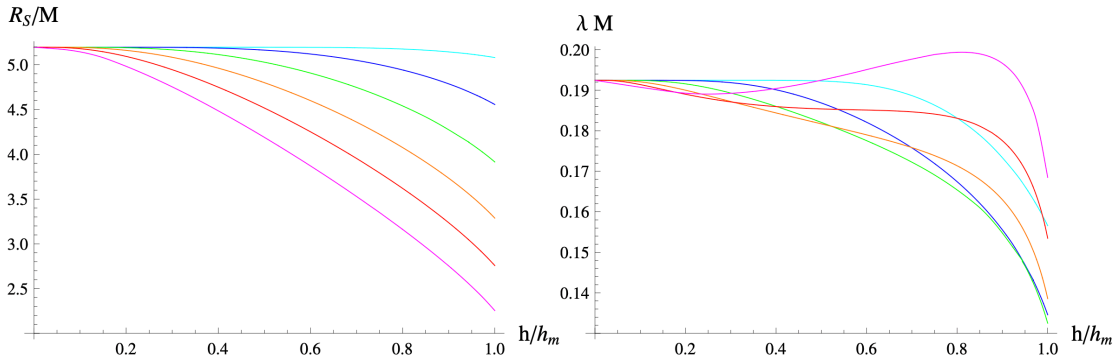

Figure 3. Shadow radius (left panel) and Lyapunov exponents (right panel) as functions of the scale parameter h in units of its maximum value h_m for the black hole solutions with Einasto profile (from top to bottom): $n = 1$ (cyan), $n = 2$ (blue), $n = 3$ (green), $n = 4$ (orange), $n = 5$ (red), $n = 6$ (magenta).

IV. Dehnen-type distributions

Another family of density profiles, which generalizes several well-known halo profiles through tunable slope parameters, is defined Dehnen[8]; Taylor and Silk[34]

$$\rho(r) = \rho_0 \left(\frac{r}{a}\right)^{-\alpha} \left(1 + \frac{r^k}{a^k}\right)^{-(\gamma-\alpha)/k}. \tag{23}$$

The density becomes infinite at $r = 0$, unless $\alpha \leq 0$. We shall also consider $\gamma > 3$, which satisfies the condition (14). Then, in order to have a monotonously decreasing profile (12), which satisfies the weak energy conditions, $\alpha = 0$. It is interesting to note that, in this case, the fluid is barotropic Sajadi *et al.*[13]. The total mass is

$$M = \frac{4\pi\rho_0 a^3 \Gamma\left(1+3/k\right)\Gamma\left(\gamma/k-3/k\right)}{3\Gamma\left(\gamma/k\right)}. \tag{24}$$

Again, for sufficiently small values of a/M, the solution possesses an event horizon.

It is noteworthy that, although for $\gamma = 3$ the total mass (24) diverges, the corresponding solutions remain asymptotically flat, whereas for $\gamma = 2$ they are asymptotically characterized by a solid angle defect (see Kar and Kar[11] for a review).

The obtained model describes a finite-density core that gradually steepens at large radii, ensuring a rapidly decaying outer halo. Although the density profile does not reproduce the standard models, such as Hernquist or NFW profiles, it represents a family of dark matter distributions with a flat asymptotic region and finite total mass. The analytic form of the line element provides a tractable framework for studying how dark matter affects the local geometry around the regular black hole.

In particular, for $k = 1$ one obtains a relatively simple expression,

$$\begin{aligned} f(r) = 1 - \frac{2m(r)}{r} &= 1 - \frac{2M}{r} \\ &+ \frac{2M}{r}\left(\frac{a}{a+r}\right)^{\gamma-3}\left(1 + \frac{(\gamma-1)(2a+\gamma r)r}{2(a+r)^2}\right). \end{aligned} \tag{25}$$

where

$$M = \frac{8\pi\rho_0 a^3}{(\gamma-3)(\gamma-2)(\gamma-1)}. \tag{26}$$

The Ricci scalar and the Kretschmann scalar for the above metric read

$$\begin{aligned} R &= \frac{M(4a-(\gamma-4)r)(\gamma-3)(\gamma-2)(\gamma-1)a^{\gamma-3}}{(a+r)^{\gamma+1}}, \\ R_{\mu\nu\lambda\sigma}R^{\mu\nu\lambda\sigma} &= \frac{8M^2(\gamma-3)^2(\gamma-2)^2(\gamma-1)^2}{3a^6} + \mathcal{O}(r). \end{aligned}$$

For $\gamma = 4$ the metric function (IV) reads

$$f(r) = 1 - \frac{2m(r)}{r} = 1 - \frac{2Mr^2}{(r+a)^3}. \tag{27}$$

For $\gamma = 4$ and $k = 2$, we have a regular black hole solution, which can be obtained within nonlinear electrodynamics minimally coupled to gravity Dymnikova[35].

Another simple solution we obtain for $k = 3$,

$$f(r) = 1 - \frac{2m(r)}{r} = 1 - \frac{2M}{r} + \frac{2M}{r}\left(1 + \frac{r^3}{a^3}\right)^{1-\gamma/3}, \tag{28}$$

where

$$M = \frac{4\pi\rho_0 a^3}{\gamma - 3}. \tag{29}$$

The curvature invariants for the above metric are

$$R = \frac{2M(\gamma-3)\left(4a^3 - r^3(\gamma-4)\right)}{a^6}\left(1+\frac{r^3}{a^3}\right)^{-1-\gamma/3},$$
$$R_{\mu\nu\lambda\sigma}R^{\mu\nu\lambda\sigma} = \frac{32M^2(\gamma-3)^2}{3a^6} + \mathcal{O}(r)^3.$$

For $\gamma = 4$ we obtain the solution (3.18) of Kar and Kar[11]. For $\gamma = 6$ the solution (28) coincides with the Hayward black hole Hayward[2].

V. Axial perturbations

In Chakraborty *et al.*[36] two types of linear axial (odd) perturbations of the spherically symmetric configurations with anisotropic fluid have been derived. In both cases the perturbation equations can be reduced to the wave-like form:

$$\frac{d^2\Psi}{dr_*^2} + \left(\omega^2 - V(r)\right)\Psi = 0, dr_* \equiv \frac{dr}{f(r)}. \tag{30}$$

The “up” perturbations correspond to the the choice of the observer, which does not see a variation in the contravariant components of the fluid and the “down” perturbations correspond the absence of the variations in the covariant components. The corresponding effective potentials are different:

$$V^{(\mathrm{up})}(r) = f(r)\left(\frac{\ell(\ell+1)}{r^2} - \frac{6m(r)}{r^3} + 4\pi\left[\rho(r) - 5P_r(r) + 4P(r)\right]\right), \tag{31}$$
$$V^{(\mathrm{down})}(r) = f(r)\left(\frac{\ell(\ell+1)}{r^2} - \frac{6m(r)}{r^3} + 4\pi\rho(r) - 4\pi P_r(r)\right). \tag{32}$$

Taking into account the condition (8) and (10) we find

$$V^{(\mathrm{up})}(r) = f(r)\left(\frac{\ell(\ell+1)}{r^2} - \frac{6m(r)}{r^3} + 8\pi\rho(r) - 8\pi r\rho'(r)\right), \tag{33}$$
$$V^{(\mathrm{down})}(r) = f(r)\left(\frac{\ell(\ell+1)}{r^2} - \frac{6m(r)}{r^3} + 8\pi\rho(r)\right).$$

Since $\rho(r) > 0$ and $\rho'(r) < 0$, both effective potentials are positive definite outside the event horizon (as $2m(r) \leq r$) for $\ell \geq 2$. Thus, the differential operator

$$\mathcal{D} = -\frac{\partial^2}{\partial r_*^2} + V(r) \tag{34}$$

is a positive self-adjoint operator in the Hilbert space of square integrable functions of r_*. Therefore, all solutions of the perturbation equations with compact support initial conditions are bounded Konoplya and Zhidenko[37], that is, the configuration is stable against axial-type gravitational perturbations.

VI. Black–hole shadow and Lyapunov exponent

One of the most important observable characteristics of a black hole surrounded by its galactic environment is the radius of its shadow. Consequently, a substantial body of research has been devoted to studying black hole shadows in various theories of gravity and for different types of surrounding matter and environments (see [38][39][40][41][42][43][44][45][46][47][48][49][50][51][52][53][54][55][56][57][58][59][60][61] and literature therein for reviews and recent examples).

The timelike and axial Killing vectors yield the conserved energy and angular momentum

$$E \equiv f(r)\frac{dt}{d\lambda}, L \equiv r^2\frac{d\phi}{d\lambda}, \tag{35}$$

with λ an affine parameter. Using $ds^2 = 0$ for null rays in the equatorial plane $\theta = \pi/2$,

$$0 = -f(r)\left(\frac{dt}{d\lambda}\right)^2 + \frac{B^2(r)}{f(r)}\left(\frac{dr}{d\lambda}\right)^2 + r^2\left(\frac{d\phi}{d\lambda}\right)^2, \tag{36}$$

one finds the radial equation

$$\left(\frac{dr}{d\lambda}\right)^2 = \frac{E^2}{B^2(r)}\left[1 - \frac{f(r)b^2}{r^2}\right], b \equiv \frac{L}{E}, \tag{37}$$

where b is the (asymptotic) impact parameter.

Null circular orbit satisfies the following relation

$$\frac{dr}{d\lambda} = 0 \quad \Longrightarrow \quad b^2 = \frac{r^2}{f(r)}. \tag{38}$$

Extremizing the impact parameter we obtain the photon sphere radius, r_{ph}, as the solution of the following equation

$$\left.\frac{db}{dr}\right|_{r=r_{ph}} = 0 \Longleftrightarrow r_{ph}f'(r_{ph}) - 2f(r_{ph}) = 0. \tag{39}$$

The corresponding *critical impact parameter* coincides with shadow radius for an observer at infinity,

$$R_S = b|_{r=r_{ph}} = \frac{r_{ph}}{\sqrt{f(r_{ph})}}. \tag{40}$$

Notice that $B(r)$ drops out of Eqs. (39) and (40); only $f(r)$ determines the photon sphere and the shadow radius R_S.

By substituting $r = r_{ph} + \delta r$ into (36) we obtain the equation for the radial coordinate of the photons that are leaving the circular orbit,

$$\left(\frac{d}{dt}\delta r\right)^2 = \lambda^2 \delta r^2 + \mathcal{O}(\delta r)^3, \tag{41}$$

where λ is the the Lyapunov exponent, satisfying,

$$\lambda^2 = -\frac{r^2 f(r)}{2B^2(r)} \frac{d^2}{dr^2} \frac{f(r)}{r^2}\bigg|_{r=r_{ph}}. \tag{42}$$

Note that $B(r) = 1$ for all the configurations considered in the present paper because of the condition (9).

For large n the Einasto density profile must be very dense and decays relatively slowly. Therefore, the black-hole metric is significantly different from the Schwarzschild geometry within the parametric range of h providing the existence of the event horizon (see Fig. 2). As a result for larger n the shadow radius and Lyapunov exponents generally differ more from their Schwarzschild values (see Fig. 3).

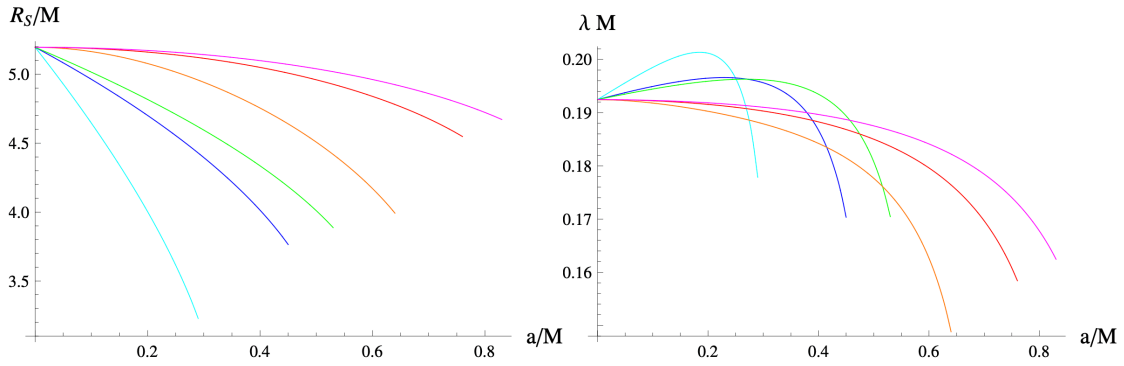

Figure 4. Shadow radius (left panel) and Lyapunov exponents (right panel) as functions of the scale parameter a for the black hole solutions with Dehnen-type profiles for $\alpha = 0$ (from shorter to longer region of a): $\gamma = 4, k = 1$ (cyan), $\gamma = 4, k = 2$ (blue), $\gamma = 4, k = 3$ (green), $\gamma = 5, k = 1$ (orange), $\gamma = 5, k = 2$ (red), $\gamma = 5, k = 3$ (magenta).

doi.org/10.32388/OHSoHC

For Dehnen-type profiles with $\alpha = 0$ (see Fig. 4), the halo density is higher for smaller values of γ and also slightly increases as the parameter k decreases. Consequently, the range of black hole shadow radii becomes larger for smaller γ and k, whereas the presence of the event horizon is observed as the scale parameter a varies within a comparatively narrower interval. In contrast, the Lyapunov exponent exhibits a broader variation range for higher values of γ, indicating stronger sensitivity of the photon orbit stability to changes in the halo profile.

It should be noted that the computed shadow radii and Lyapunov exponents can also be used to estimate quasinormal modes in the eikonal (high-multipole) limit through the well-known correspondence between the orbital frequency/shadow's radius of the circular null geodesic and the real part of the quasinormal frequency, as well as between the Lyapunov exponent and the damping rate Cardoso *et al.* [62]; Jusufi[63]. Although several exceptions to this correspondence have been identified in Konoplya and Stuchlík[64]; Khanna and Price[65]; Konoplya[66]; Bolokhov[67]; Konoplya and Zinhailo[68]; Konoplya *et al.*[69], the present wave equation exhibits proper WKB eikonal behavior, ensuring that the correspondence remains valid in our case.

VII. Discussions

It is important to emphasize that, once we assume that $m(0) = 0$ in (11), the considered solutions always have a de Sitter core,

$$f(r) = 1 - \frac{2m(r)}{r} = 1 - \frac{8\pi\rho_0}{3}r^2 + \mathcal{O}(r)^3. \tag{43}$$

Therefore, the Ricci scalar and Kretschmann scalar,

$$\begin{aligned} R &= -f''(r) - \frac{4}{r}f'(r) + \frac{2\left(1 - f(r)\right)}{r^2}, \\ R_{\mu\nu\lambda\sigma}R^{\mu\nu\lambda\sigma} &= f''(r)^2 + \frac{4}{r^2}f'(r)^2 + \frac{4}{r^4}\left(1 - f(r)\right)^2, \end{aligned} \tag{44}$$

are regular at $r = 0$.

The general static spherically symmetric solution of the Einstein equations discussed in Sec. IIcan be parametrized by the arbitrary constant $m(0) = m_0$. The resulting metric function $\widetilde{f}(r)$ can be expressed as follows:

$$\widetilde{f}(r) = f(r) - \frac{2m_0}{r}, \tag{45}$$

leading to a singular family of black holes with only one regular solution corresponding to $m_0 = 0$. A similar observation has been made for the Bardeen and Hayward black holes as solutions within nonlinear electrodynamics Huang and Rao[70]. Energy conditions of singular black holes immersed in various models of dark matter halo, including the Einasto and Dehnan density profiles, were analyzed in Datta[71].

In order to regard regular black holes supported by a dark-matter halo as astrophysically plausible, one must assume that such halo configurations could have existed already during the epoch of stellar collapse. In standard scenarios of stellar evolution, the baryonic density of the collapsing star vastly exceeds the local density of dark matter, so the latter is not expected to dominate the collapse dynamics. Nevertheless, cosmological N-body simulations in the ΛCDM paradigm predict that galaxies and their progenitors formed within extended dark matter halos Navarro *et al.*[4]; Springel *et al.*[72], implying that any stellar collapse took place in an environment permeated by dark matter. Moreover, in the early Universe dark matter over densities or self-interacting dark matter models may have led to locally enhanced densities Spergel and Steinhardt[73]; Tulin and Yu[74], while compact dark matter structures such as solitonic cores or spikes around primordial black holes could also provide significant local contributions Gondolo and Silk[75]; Ullio *et al.*[76]. Regular primordial black holes, in their turn, can act as cosmic expansion accelerators Dialektopoulos *et al.*[77]. Even if dark matter did not directly drive the collapse, subsequent accretion from the ambient halo can build up dense distributions around newly formed black holes Bertone *et al.*[5]. Thus, although baryonic matter is the primary agent in stellar collapse, there exist several physically motivated scenarios in which dark matter halos may consistently act as effective sources in constructing regular black-hole geometries.

VIII. Conclusions

In this work we have constructed exact black hole solutions free from curvature singularities, sourced by a galactic dark-matter halo. The regularity of these geometries follows from the specific relation $P_r = -\rho$ between radial pressure and density, which is consistent with the phenomenological freedom in halo modeling. The regular black hole solution is shown to be stable against axial perturbations. While this could be an indication that the solution is stable, the full analysis of stability must also include the polar type of perturbations. The obtained solutions demonstrate that halo distributions can serve not only as astrophysical environments but also as effective sources of singularity resolution. The radius of

shadow and the Lyapunov exponent for circular null geodesics are discussed for particular examples of regular black holes.

A natural direction for further study is the investigation of physical observables associated with these regular configurations[78]. In particular, the analysis of gravitational spectra through quasinormal modes and echoes can provide insights into the stability and response of such black holes under perturbations. Similarly, the study of electromagnetic spectra, including gravitational lensing[79], and energy emission, offers potential observational signatures that could distinguish regular black holes embedded in halos from their singular Schwarzschild or Kerr counterparts.

The literature on singular black holes surrounded by galactic halos is already extensive, covering quasinormal ringing Konoplya[80]; Konoplya and Zhidenko[15]; Dubinsky[81]; Feng and Zhang[82]; Pezzella *et al.*[83]; Chakraborty *et al.*[36]; Liu *et al.*[84][85]; Zhao *et al.*[86]; Daghigh and Kunstatter[87]; Zhang *et al.*[88], grey-body factors Hamil *et al.*[89]; Mollicone and Destounis[90]; Tovar *et al.*[91]; Lütfüoğlu[92]; Pathrikar[93], black hole shadows and lensing Konoplya *et al.*[94]; Hou *et al.*[95]; Kouniatalis *et al.*[96]; Fernandes and Cardoso[97]; Chen *et al.*[98]; Tan *et al.*[99]; Macedo *et al.*[100]; Xavier *et al.*[101]; Figueiredo *et al.*[102]; Konoplya *et al.*[103], and dynamical processes such as accretion Chowdhury *et al.*[104]; Heydari-Fard *et al.*[105]. Extending these analyses to the case of regular black holes supported by halo matter would allow one to quantify the extent to which regularity alters these spectra and potentially leaves imprints observable with current or near-future instruments.

Notes

PACS: 04.70.Bw,95.35.+d,98.62.Js.

References

1. ^*Bardeen JM (1968). Proceedings of the International Conference GR5.*
2. a, b *Hayward SA (2006). "Formation and Evaporation of Nonsingular Black Holes." Phys Rev Lett.* **96***(3):031103. doi:10.1103/physrevlett.96.031103.*
3. ^*Ansoldi S (2008). "Conference on Black Holes and Naked Singularities."*
4. a, b, c *Navarro JF, Frenk CS, White SDM (1997). "A Universal Density Profile from Hierarchical Clustering." Astrophys J.* **490***:493. doi:10.1086/304888.*

5. ^a, ^b*Bertone G, Hooper D, Silk J (2005). "Particle Dark Matter: Evidence, Candidates and Constraints." Phys R ept.* ***405****:279. doi:10.1016/j.physrep.2004.08.031.*
6. ^*Hernquist L (1990). "An Analytical Model for Spherical Galaxies and Bulges." Astrophys J.* ***356****:359. doi:10.10 86/168845.*
7. ^*Einasto J (1965). "Trudy Astrofizicheskogo Instituta Alma-Ata." Trudy Astrofizicheskogo Instituta Alma-At a.* ***5****:87.*
8. ^a, ^b*Dehnen W (1993). "Mon. Not. Roy. Astron. Soc." Mon Not Roy Astron Soc.* ***265****:250.*
9. ^*Dekel A, Ishai G, Dutton AA, Maccio AV (2017). "Dark-Matter Halo Profiles of a General Cusp/Core with An alytic Velocity and Potential." Mon Not Roy Astron Soc.* ***468****:1005. doi:10.1093/mnras/stx486.*
10. ^*Zhao H (1996). "Analytical Models for Galactic Nuclei." Mon Not Roy Astron Soc.* ***278****:488. doi:10.1093/mnra s/278.2.488.*
11. ^a, ^b, ^c*Kar A, Kar S (2025). "Diverse Regular Spacetimes Using a Parametrised Density Profile." Eur Phys J C.* ***8 5****:773. doi:10.1140/epjc/s10052-025-14483-5.*
12. ^*Sajadi SN, Khodadi M, Luongo O, Quevedo H (2024). "Anisotropic Generalized Polytropic Spheres: Regular 3D Black Holes." Phys Dark Univ.* ***45****:101525. doi:10.1016/j.dark.2024.101525.*
13. ^a, ^b*Sajadi SN, Ponglertsakul S, Luongo O (2025). "Constructing Black Holes from Multi-Polytropic Equations of State." Phys Dark Univ.* ***48****:101938. doi:10.1016/j.dark.2025.101938.*
14. ^*Benson AJ (2010). "Galaxy Formation Theory." Phys Rept.* ***495****:33. doi:10.1016/j.physrep.2010.06.001.*
15. ^a, ^b*Konoplya RA, Zhidenko A (2022). "Solutions of the Einstein Equations for a Black Hole Surrounded by a Galactic Halo." Astrophys J.* ***933****:166. doi:10.3847/1538-4357/ac76bc.*
16. ^*Zaslavskii OB (2025).*
17. ^*Kamenshchik AY, Moschella U, Pasquier V (2001). "Phys. Lett. B." Phys Lett B.* ***511****:265.*
18. ^*Bento MC, Bertolami O, Sen AA (2002). "Phys. Rev. D." Phys Rev D.* ***66****:043507.*
19. ^*Scherrer RJ (2004). "Phys. Rev. Lett." Phys Rev Lett.* ***93****:011301.*
20. ^*Dymnikova I, Khlopov M (2015). "Regular Black Hole Remnants and Graviatoms with De Sitter Interior as Heavy Dark Matter Candidates Probing Inhomogeneity of Early Universe." Int J Mod Phys D.* ***24****:1545002. d oi:10.1142/S0218271815450029.*
21. ^*Balakin AB, Pavón D, Schwarz DJ, Zimdahl W (2003). "New J. Phys." New J Phys.* ***5****:85.*
22. ^*Sahni V, Shtanov Y (2003). "JCAP." JCAP.* ***0311****:014.*

23. ^ a, b *Einasto J (1965). "Trudy Astrofizicheskogo Instituta Alma-Ata" [Proceedings of the Astrophysical Institute Alma-Ata]. Trudy Astrofizicheskogo Instituta Alma-Ata [Proceedings of the Astrophysical Institute Alma-Ata]. **5**:87.*

24. ^ a, b *Einasto J, Haud U (1989). "Astronomy and Astrophysics." Astron Astrophys. **223**:89.*

25. ^ *Retana-Montenegro E, Van Hese E, Gentile G, Baes M, Frutos-Alfaro F (2012). "Analytical Properties of Einasto Dark Matter Haloes." Astron Astrophys. **540**:A70. doi:10.1051/0004-6361/201118543.*

26. ^ *Baes M (2022). "The Einasto Model for Dark Matter Haloes." Astron Astrophys. **667**:A47. doi:10.1051/0004-6361/202244567.*

27. ^ *Merritt D, Navarro JF, Ludlow A, Jenkins A (2006). "Astronomical Journal." Astron J. **132**:2685.*

28. ^ *Navarro JF, et al. (2004). "Monthly Notices of the Royal Astronomical Society." Mon Not Roy Astron Soc. **349**:1039.*

29. ^ *Springel V, et al. (2008). "Monthly Notices of the Royal Astronomical Society." Mon Not Roy Astron Soc. **391**:1685.*

30. ^ *Acharyya R, Banerjee P, Kar S (2024). "Modelling Einstein Cluster Using Einasto Profile." JCAP. **04**:070. doi:10.1088/1475-7516/2024/04/070.*

31. ^ *Graham AW, Merritt D, Moore B, Diemand J, Terzić B (2006). "Astrophysical Journal Letters." Astrophys J Lett. **653**:L121.*

32. ^ *Ludlow AD, Navarro JF, Angulo RE, et al. (2013). "Monthly Notices of the Royal Astronomical Society." Mon Not Roy Astron Soc. **432**:1103.*

33. ^ *Boos J (2025). "Non-Singular “Gauss” Black Hole from Non-Locality." Universe. **11**:112. doi:10.3390/universe11040112.*

34. ^ *Taylor JE, Silk J (2003). "The Clumpiness of Cold Dark Matter: Implications for the Annihilation Signal." Mon Not Roy Astron Soc. **339**:505. doi:10.1046/j.1365-8711.2003.06201.x.*

35. ^ *Dymnikova I (2004). "Regular Electrically Charged Vacuum Structures with De Sitter Centre in Nonlinear Electrodynamics Coupled to General Relativity." Class Quant Grav. **21**:4417. doi:10.1088/0264-9381/21/18/009.*

36. ^ a, b *Chakraborty S, Compère G, Machet L (2025). "Tidal Love Numbers and Quasinormal Modes of the Schwarzschild-Hernquist Black Hole." Phys Rev D. **112**:024015. doi:10.1103/4p2c-rwdh.*

37. ^ *Konoplya RA, Zhidenko A (2011). "Quasinormal Modes of Black Holes: From Astrophysics to String Theory." Rev Mod Phys. **83**:793. doi:10.1103/revmodphys.83.793.*

38. ^Cunha PVP, Herdeiro CAR (2018). "Shadows and Strong Gravitational Lensing: A Brief Review." Gen Rel Grav. **50**:42. doi:10.1007/s10714-018-2361-9.

39. ^Perlick V, Tsupko OY (2022). "Calculating Black Hole Shadows: Review of Analytical Studies." Phys Rept. **947**:1. doi:10.1016/j.physrep.2021.10.004.

40. ^Bambi C (2017). "Testing Black Hole Candidates with Electromagnetic Radiation." Rev Mod Phys. **89**:025001. doi:10.1103/revmodphys.89.025001.

41. ^Hioki K, Maeda K-i (2009). "Measurement of the Kerr Spin Parameter by Observation of a Compact Object's Shadow." Phys Rev D. **80**:024042. doi:10.1103/PhysRevD.80.024042.

42. ^Bonanno A, Konoplya RA, Oglialoro G, Spina A (2025).

43. ^Konoplya RA (2019). "Shadow of a Black Hole Surrounded by Dark Matter." Phys Lett B. **795**:1. doi:10.1016/j.physletb.2019.05.043.

44. ^Younsi Z, Zhidenko A, Rezzolla L, Konoplya R, Mizuno Y (2016). "New Method for Shadow Calculations: Application to Parametrized Axisymmetric Black Holes." Phys Rev D. **94**:084025. doi:10.1103/PhysRevD.94.084025.

45. ^Bambi C, Freese K, Vagnozzi S, Visinelli L (2019). "Testing the Rotational Nature of the Supermassive Object M87* from the Circularity and Size of Its First Image." Phys Rev D. **100**:044057. doi:10.1103/PhysRevD.100.044057.

46. ^Konoplya RA, Ovchinnikov D, Schee J (2025).

47. ^Perlick V, Tsupko OY, Bisnovatyi-Kogan GS (2015). "Influence of a Plasma on the Shadow of a Spherically Symmetric Black Hole." Phys Rev D. **92**:104031. doi:10.1103/PhysRevD.92.104031.

48. ^Konoplya RA, Stashko OS (2025). "Probing the Effective Quantum Gravity Via Quasinormal Modes and Shadows of Black Holes." Phys Rev D. **111**:104055. doi:10.1103/physrevd.111.104055.

49. ^Khodadi M, Allahyari A, Vagnozzi S, Mota DF (2020). "Black Holes with Scalar Hair in Light of the Event Horizon Telescope." JCAP. **09**:026. doi:10.1088/1475-7516/2020/09/026.

50. ^Kumar R, Ghosh SG (2020). "Black Hole Parameter Estimation from Its Shadow." Astrophys J. **892**:78. doi:10.3847/1538-4357/ab77b0.

51. ^Konoplya RA, Zhidenko A (2021). "Shadows of Parametrized Axially Symmetric Black Holes Allowing for Separation of Variables." Phys Rev D. **103**:104033. doi:10.1103/physrevd.103.104033.

52. ^Afrin M, Kumar R, Ghosh SG (2021). "Parameter Estimation of Hairy Kerr Black Holes from Its Shadow and Constraints from M87*." Mon Not Roy Astron Soc. **504**:5927. doi:10.1093/mnras/stab1260.

53. ^Zakharov AF (2014). "Constraints on a Charge in the Reissner-Nordström Metric for the Black Hole at the Galactic Center." Phys Rev D. **90**:062007. doi:10.1103/PhysRevD.90.062007.

54. ^Zakharov AF (2025). "Shadow in the Galactic Center: Theoretical Concept – Prediction – Realization." Natural Sci Rev. **2**:100402. doi:10.54546/NaturalSciRev.100402.

55. ^Zakharov AF (2025). "Galactic Center Shadows: Beyond the Standard Model." Phys Atom Nucl. **88**:154. doi:10.1134/S106377882570019X.

56. ^Lütfüoğlu BC (2025). "Black Holes in Proca-Gauss-Bonnet Gravity with Primary Hair: Particle Motion, Shadows, and Grey-Body Factors." Int J Grav Theor Phys. **1**:4. doi:10.53941/ijgtp.2025.100004.

57. ^Konoplya RA, Pappas T, Zhidenko A (2020). "Einstein-Scalar–Gauss-Bonnet Black Holes: Analytical Approximation for the Metric and Applications to Calculations of Shadows." Phys Rev D. **101**:044054. doi:10.1103/PhysRevD.101.044054.

58. ^Konoplya RA, Zhidenko A (2019). "Analytical Representation for Metrics of Scalarized Einstein-Maxwell Black Holes and Their Shadows." Phys Rev D. **100**:044015. doi:10.1103/PhysRevD.100.044015.

59. ^Tsukamoto N (2018). "Black Hole Shadow in an Asymptotically Flat, Stationary, and Axisymmetric Spacetime: The Kerr-Newman and Rotating Regular Black Holes." Phys Rev D. **97**:064021. doi:10.1103/PhysRevD.97.064021.

60. ^Stashko O (2024). "Quasinormal Modes and Gray-Body Factors of Regular Black Holes in Asymptotically Safe Gravity." Phys Rev D. **110**:084016. doi:10.1103/physrevd.110.084016.

61. ^Spina A (2025). "Black Holes in Asymptotic Safety: A Review of Solutions and Phenomenology." Int J Grav Theor Phys. **1**:8. doi:10.53941/ijgtp.2025.100008.

62. ^Cardoso V, Miranda AS, Berti E, Witek H, Zanchin VT (2009). "Geodesic Stability, Lyapunov Exponents, and Quasinormal Modes." Phys Rev D. **79**:064016. doi:10.1103/PhysRevD.79.064016.

63. ^Jusufi K (2020). "Connection Between the Shadow Radius and Quasinormal Modes in Rotating Spacetimes." Phys Rev D. **101**:124063. doi:10.1103/PhysRevD.101.124063.

64. ^Konoplya RA, Stuchlík Z (2017). "Are Eikonal Quasinormal Modes Linked to the Unstable Circular Null Geodesics?" Phys Lett B. **771**:597. doi:10.1016/j.physletb.2017.06.015.

65. ^Khanna G, Price RH (2017). "Black Hole Ringing, Quasinormal Modes, and Light Rings." Phys Rev D. **95**:081501. doi:10.1103/PhysRevD.95.081501.

66. ^Konoplya RA (2023). "Further Clarification on Quasinormal Modes/Circular Null Geodesics Correspondence." Phys Lett B. **838**:137674. doi:10.1016/j.physletb.2023.137674.

67. ^Bolokhov SV (2024). "Black Holes in Starobinsky-Bel-Robinson Gravity and the Breakdown of Quasinormal Modes/Null Geodesics Correspondence." Phys Lett B. **856**:138879. doi:10.1016/j.physletb.2024.138879.

68. ^Konoplya RA, Zinhailo AF (2020). "Quasinormal Modes, Stability and Shadows of a Black Hole in the 4D Einstein–Gauss–Bonnet Gravity." Eur Phys J C. **80**:1049. doi:10.1140/epjc/s10052-020-08639-8.

69. ^Konoplya RA, Spina A, Zhidenko A (2025). "Time Evolution of Black Hole Perturbations in Quadratic Gravity." Phys Rev D. **112**:024060. doi:10.1103/xhtc-9cf4.

70. ^Huang H, Rao X-P (2025). "Regular Black Holes and Their Singular Families." Phys Rev D. **111**:104040. doi:10.1103/physrevd.111.104040.

71. ^Datta S (2024). "Black Holes Immersed in Dark Matter: Energy Condition and Sound Speed." Phys Rev D. **109**:104042. doi:10.1103/physrevd.109.104042.

72. ^Springel V, et al. (2005). "Simulations of the Formation, Evolution and Clustering of Galaxies and Quasars." Nature. **435**:629. doi:10.1038/nature03597.

73. ^Spergel DN, Steinhardt PJ (2000). "Observational Evidence for Self-Interacting Cold Dark Matter." Phys Rev Lett. **84**:3760. doi:10.1103/PhysRevLett.84.3760.

74. ^Tulin S, Yu H-B (2018). "Dark Matter Self-Interactions and Small Scale Structure." Phys Rept. **730**:1. doi:10.1016/j.physrep.2017.11.004.

75. ^Gondolo P, Silk J (1999). "Dark Matter Annihilation at the Galactic Center." Phys Rev Lett. **83**:1719. doi:10.1103/PhysRevLett.83.1719.

76. ^Ullio P, Zhao H, Kamionkowski M (2001). "Dark-Matter Spike at the Galactic Center?" Phys Rev D. **64**:043504. doi:10.1103/PhysRevD.64.043504.

77. ^Dialektopoulos K, Papanikolaou T, Zarikas V (2025). "Primordial Black Holes as Cosmic Expansion Accelerators." Phys Lett B. **870**:139948. doi:10.1016/j.physletb.2025.139948.

78. ^Vagnozzi S, et al. (2023). "Horizon-Scale Tests of Gravity Theories and Fundamental Physics from the Event Horizon Telescope Image of Sagittarius A*." Class Quant Grav. **40**:165007. doi:10.1088/1361-6382/acd97b.

79. ^Boos J, Hu H (2025).

80. ^Konoplya RA (2021). "Black Holes in Galactic Centers: Quasinormal Ringing, Grey-Body Factors and Unruh Temperature." Phys Lett B. **823**:136734. doi:10.1016/j.physletb.2021.136734.

81. ^Dubinsky A (2025). "Int. J. Grav. Theor. Phys." Int J Grav Theor Phys. **1**:2.

82. ^Feng X-H, Zhang G-Y (2025).

83. ^Pezzella L, Destounis K, Maselli A, Cardoso V (2025). "Quasinormal Modes of Black Holes Embedded in Halos of Matter." Phys Rev D. **111**:064026. doi:10.1103/PhysRevD.111.064026.

84. ^Liu Y, Mu B, Tao J, Weng Y (2025). "Quasinormal Modes of Schwarzschild-Like Black Hole Surrounded by the Pseudo-Isothermal Dark Matter Halo." Nucl Phys B. **1010**:116787. doi:10.1016/j.nuclphysb.2024.116787.

85. ^Liu D, Yang Y, Long Z-W (2024). "Probing Black Holes in a Dark Matter Spike of M87 Using Quasinormal Modes." Eur Phys J C. **84**:731. doi:10.1140/epjc/s10052-024-13096-8.

86. ^Zhao Y, Sun B, Lin K, Cao Z (2023). "Axial Gravitational Ringing of a Spherically Symmetric Black Hole Surrounded by Dark Matter Spike." Phys Rev D. **108**:024070. doi:10.1103/PhysRevD.108.024070.

87. ^Daghigh RG, Kunstatter G (2022). "Spacetime Metrics and Ringdown Waveforms for Galactic Black Holes Surrounded by a Dark Matter Spike." Astrophys J. **940**:33. doi:10.3847/1538-4357/ac940b.

88. ^Zhang C, Zhu T, Wang A (2021). "Gravitational Axial Perturbations of Schwarzschild-Like Black Holes in Dark Matter Halos." Phys Rev D. **104**:124082. doi:10.1103/PhysRevD.104.124082.

89. ^Hamil B, Al-Badawi A, Lütfüoğlu BC (2025).

90. ^Mollicone A, Destounis K (2025). "Superradiance of Charged Black Holes Embedded in Dark Matter Halos." Phys Rev D. **111**:024017. doi:10.1103/PhysRevD.111.024017.

91. ^Tovar LOT, Pedraza O, López LA, Arceo R (2025).

92. ^Lütfüoğlu BC (2025).

93. ^Pathrikar A (2025).

94. ^Konoplya RA, Stuchlík Z, Zhidenko A (2025). "Charged Black Hole Surrounded by a Galactic Halo in a De Sitter Universe." Phys Rev D. **112**:083014. doi:10.1103/l33g-6hlr.

95. ^Hou X, Xu Z, Wang J (2018). "Rotating Black Hole Shadow in Perfect Fluid Dark Matter." JCAP. **12**:040. doi:10.1088/1475-7516/2018/12/040.

96. ^Kouniatalis G, Suvorov AG, Destounis K (2025).

97. ^Fernandes PGS, Cardoso V (2025).

98. ^Chen R-Y, Javed F, Mustafa DG, Maurya SK, Ray S (2024). "Dual Effect of String Cloud and Dark Matter Halos on Particle Motions, Shadows and Epicyclic Oscillations Around Schwarzschild Black Holes." JHEAp. **44**:172. doi:10.1016/j.jheap.2024.09.010.

99. ^Tan Q, Deng W, Long S, Jing J (2025). "Motion of Spinning Particles Around Black Hole in a Dark Matter Halo." JCAP. **05**:044. doi:10.1088/1475-7516/2025/05/044.

100. ^Macedo CFB, Rosa JL, Rubiera-Garcia D (2024). "Optical Appearance of Black Holes Surrounded by a Dark Matter Halo." JCAP. **07**:046. doi:10.1088/1475-7516/2024/07/046.

101. ^Xavier SVMCB, Lima Junior HCD, Crispino LCB (2023). "Shadows of Black Holes with Dark Matter Halo." Phys Rev D. **107**(6):064040. doi:10.1103/physrevd.107.064040.

102. ^Figueiredo E, Maselli A, Cardoso V (2023). "Black Holes Surrounded by Generic Dark Matter Profiles: Appearance and Gravitational-Wave Emission." Phys Rev D. **107**(10):104033. doi:10.1103/physrevd.107.104033.

103. ^Konoplya RA, Khrabustovskyi A, Kříž J, Zhidenko A (2025). "Quasinormal Ringing and Shadows of Black Holes and Wormholes in Dark Matter-Inspired Weyl Gravity." J Cosmol Astropart Phys. **2025**(04):062. doi:10.1088/1475-7516/2025/04/062.

104. ^Chowdhury A, Sen G, Chakrabarti S, Das S (2025). arXiv:2503.08528 [gr-qc].

105. ^Heydari-Fard M, Heydari-Fard M, Riazi N (2025). "Galactic Black Hole Immersed in a Dark Halo with Its Surrounding Thin Accretion Disk." Gen Relativ Gravit. **57**(2):49. doi:10.1007/s10714-025-03382-5.

Declarations

Funding: Conselho Nacional de Desenvolvimento Científico e Tecnológico (CNPq)

Potential competing interests: No potential competing interests to declare.